PCCP

PAPER

View Article Online
View Journal

Cite this: DOI: 10.1039/c5cp03671b

Pulsed EPR dipolar spectroscopy at Q- and G-band on a trityl biradical†

D. Akhmetzyanov,‡[a] P. Schöps,‡[a] A. Marko,[a] N. C. Kunjir,[b] S. Th. Sigurdsson*[b] and T. F. Prisner*[a]

Received 24th June 2015,
Accepted 24th August 2015

DOI: 10.1039/c5cp03671b

www.rsc.org/pccp

Pulsed electron paramagnetic resonance (EPR) spectroscopy is a valuable technique for the precise determination of distances between paramagnetic spin labels that are covalently attached to macromolecules. Nitroxides have commonly been utilised as paramagnetic tags for biomolecules, but trityl radicals have recently been developed as alternative spin labels. Trityls exhibit longer electron spin relaxation times and higher stability than nitroxides under *in vivo* conditions. So far, trityl radicals have only been used in pulsed EPR dipolar spectroscopy (PDS) at X-band (9.5 GHz), K_u-band (17.2 GHz) and Q-band (34 GHz) frequencies. In this study we investigated a trityl biradical by PDS at Q-band (34 GHz) and G-band (180 GHz) frequencies. Due to the small spectral width of the trityl (30 MHz) at Q-band frequencies, single frequency PDS techniques, like double-quantum coherence (DQC) and single frequency technique for refocusing dipolar couplings (SIFTER), work very efficiently. Hence, Q-band DQC and SIFTER experiments were performed and the results were compared; yielding a signal to noise ratio for SIFTER four times higher than that for DQC. At G-band frequencies the resolved axially symmetric ***g***-tensor anisotropy of the trityl exhibited a spectral width of 130 MHz. Thus, pulsed electron electron double resonance (PELDOR/DEER) obtained at different pump–probe positions across the spectrum was used to reveal distances. Such a multi-frequency approach should also be applicable to determine structural information on biological macromolecules tagged with trityl spin labels.

Introduction

Triarylmethyl based radicals (TAM or trityl)[1] have attracted considerable attention in electron paramagnetic resonance (EPR) applications, particularly in EPR imaging[2] and pulsed EPR dipolar spectroscopy (PDS) as spin probes.[3–7] These types of carbon centred radicals have several unique properties, such as a narrow spectral width, long electron spin relaxation times (even at ambient temperatures)[8–10] as well as high stability toward redox processes.[2] These features make the utilisation of trityl radicals in EPR useful, especially for PDS applications under physiological[3,4] and *in vivo* conditions.

PDS enables the determination of nanometer-scale distances between two specifically attached spin probes through the magnitude of their magnetic dipole–dipole coupling. Hence, important information about structure, conformational changes and folding of large biomolecules can be obtained.[11,12] The choice of PDS technique should depend on the type of paramagnetic spin probes that are being used. In the case of paramagnetic centres which have EPR spectra that are significantly broader than the excitation bandwidth of the available microwave pulses, pulsed electron electron double resonance (PELDOR,[13,14] also called DEER[15,16]) is very robust, efficient and hence the most widely used PDS technique. Most commonly, a pair of nitroxide radicals, incorporated into the molecule of interest by site-directed spin labelling, has been used for these type of experiments.[17–21] On the other hand, if the excitation bandwidth of the available microwave pulses is large enough to excite the whole EPR spectrum, *e.g.* in case of trityls, the usage of single frequency techniques like double-quantum coherence (DQC),[22] or the single frequency technique for refocusing dipolar couplings (SIFTER)[23] is preferred due to higher sensitivity. Achieving this condition for nitroxides is non-trivial, due to their broad EPR spectra, although this limitation has been overcome using broadband shaped microwave pulses in a SIFTER experiment at X-band frequencies[24] and very short rectangular pulses for DQC at X- and K_u-band frequencies.[22,25]

[a] *Goethe-University Frankfurt am Main, Institute of Physical and Theoretical Chemistry and Center for Biomolecular Magnetic Resonance, Max von Laue Str. 7, 60438 Frankfurt am Main, Germany. E-mail: prisner@chemie.uni-frankfurt.de*
[b] *University of Iceland, Department of Chemistry, Science Institute, Dunhaga 3, 107 Reykjavik, Iceland. E-mail: snorrisi@hi.is*

† Electronic supplementary information (ESI) available: Chemical structure of monoradical **2**. EPR spectrum of monoradical **2** and comparison with the spectrum of biradical **1**. Q-band SIFTER and DQC raw time traces of biradical **1** with the background functions. G-band PELDOR raw time traces of biradical **1** with the background functions. Simulating the PELDOR time traces using PELDOR database approach. See DOI: 10.1039/c5cp03671b

‡ Authors contributed equally to the work.

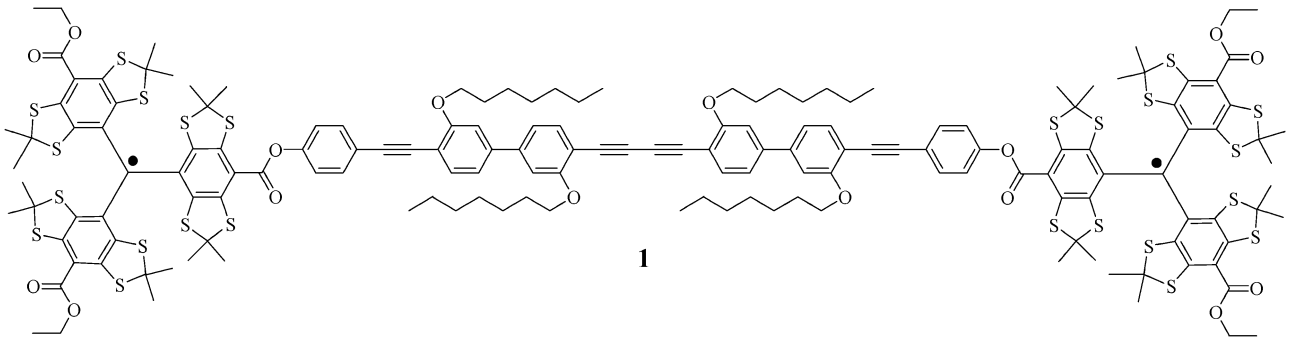

1

Fig. 1 Chemical structure of biradical **1**.

In contrast to nitroxides, trityl radicals have a significantly narrower EPR spectrum and even rectangular pulses with moderate power at X-[5,6] and Q-band frequencies can be used to excite their whole EPR spectrum. However, the width of the trityl EPR spectrum exceeds the excitation bandwidth of the available microwave pulses considerably at higher frequencies. This prefers PELDOR experiments with trityl radicals to be performed. As the EPR spectral width of trityls is significantly narrower compared to nitroxides, the sensitivity of comparable PELDOR experiments is greater for trityls.

Despite the aforementioned advantages of trityl-based radicals, only a few examples for PDS applications on biological systems[3,4,7] as well as methodological PDS studies using X-band frequencies[5,6] have been presented thus far. In the current study we investigate and describe PDS experiments on a trityl biradical **1** (Fig. 1) at Q (33.8 GHz) and G (180 GHz) – band frequencies. The results of SIFTER and DQC experiments at Q-band frequencies were compared. In addition, PELDOR experiments on biradical **1** were performed at G-band frequencies. The PELDOR time traces obtained at different pump–probe positions across the EPR spectrum exhibited orientation selection. Averaging two G-band time traces allowed Tikhonov regularisation[26] to be used to extract a distance distribution. Similar distance distributions were also obtained from the Q-band SIFTER and DQC experiments.

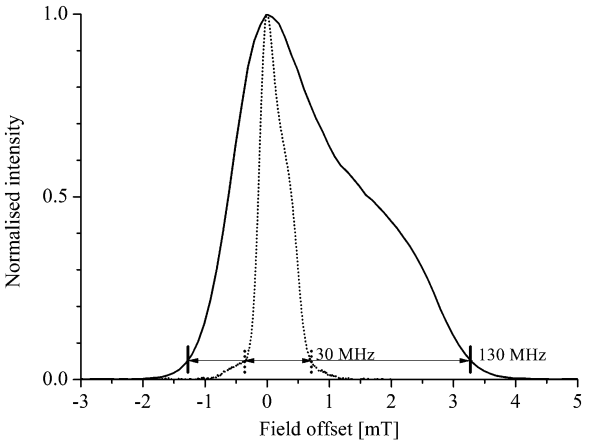

Fig. 2 Field-swept Hahn echo-detected EPR spectrum of biradical **1** obtained at Q-band frequencies at a temperature of 50 K (dotted line) and at G-band frequencies at a temperature of 25 K (solid line). The axis of abscissas corresponds to the field offset from the maximum absorption position in the spectrum. The parallel bars indicate the width of the EPR spectra.

Results and discussion

Trityl biradical 1

The trityl biradical **1**, possessing a distance between the unpaired electrons of about 4.89 nm, was synthesised according to the previously published protocol.[6]

EPR spectroscopy

Field-swept Hahn echo-detected EPR spectra of biradical 1 at Q- and G-band frequencies

The field-swept Hahn echo-detected EPR spectra of biradical **1** obtained at Q- and G-band frequencies are shown in Fig. 2. The EPR spectrum obtained at Q-band frequencies reveals a relatively narrow line with a spectral width of about 30 MHz, defined by the signal at greater than 5% echo intensity. This neglects the two weak ^{13}C satellites (including these satellites the width of the EPR spectrum is about 55 MHz). The EPR spectrum obtained at G-band frequencies shows a spectral width of about 130 MHz. The more pronounced asymmetry of the G-band EPR spectrum is due to the partially resolved ***g***-tensor anisotropy. The fact that the width of the trityl EPR spectrum scales with the microwave frequency indicates that the primary contribution to the width is the ***g***-tensor anisotropy.

The G-band field-swept Hahn echo-detected EPR spectrum of the trityl monoradical **2** (Fig. S1, ESI†) also revealed a ***g***-tensor anisotropy but with a slightly narrower spectral width of approximately 120 MHz (Fig. S2 and S3, ESI†). It is worth noting, that small changes in the chemical structure of the trityl moiety can lead to a significant change in the width of the EPR spectra and the principal values of the ***g***-tensor.[9,10,27–29]

SIFTER and DQC at Q-band frequencies

The background-corrected time traces obtained with SIFTER (Fig. 3 left) and DQC (Fig. 3 right) on biradical **1** show clear dipolar oscillations. This indicates that the biradical possess a relatively rigid structure. The raw experimental SIFTER and DQC time traces are presented in Fig. S4 (ESI†) with the corresponding background functions.

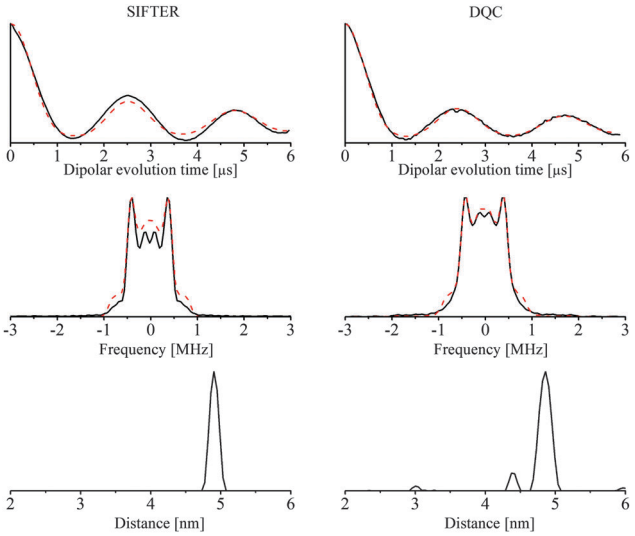

Fig. 3 Top. Background-corrected SIFTER (left) and DQC (right) time traces obtained at Q-band frequencies and a temperature of 50 K. The solid lines are experimental time traces and the dashed lines are the fits obtained by Tikhonov regularisation with the regularisation parameter of 0.1 using DeerAnalysis software.[26] The axes of ordinates are not shown, since the background-correction procedure was different for the experiments so that the *y*-axes-scaling is arbitrary in this term. For more detailed information the reader is referred to Fig. S4 (ESI†). Middle. Fourier transformation of the background-corrected SIFTER (left) and DQC (right) time traces. The solid lines are the transformation of the experimental time traces and the dashed lines are transformations of the fitted time traces. All Pake patterns are normalised. Bottom. Distance distribution functions obtained from SIFTER (left side) and DQC (right sight) time traces with Tikhonov regularisation fit.

The dipole–dipole coupling is given by the formula:[15]

$$\omega_{AB} = \frac{\mu_B{}^2 g_A g_B}{\hbar}\frac{1}{R^3}\left(3\cos^2(\theta) - 1\right) = D \cdot \left(3\cos^2(\theta) - 1\right) \quad (1)$$

where μ_B is the Bohr magneton, $\hbar$ is the Planck constant divided by 2π, g_A and g_B are the effective values of the ***g***-tensor corresponding to the excited A and B spins, R is the electron–electron distance and θ is the angle between the vector ***R*** and the external magnetic field $\boldsymbol{B}_0$. The long period of the dipolar oscillation implies a relatively large distance between the intramolecular spins.[5,6] Thus, the major part of the intramolecular spins A and B in the ensemble have a resonance frequencies difference $|\omega_A - \omega_B|$, which exceeds the absolute value of the dipole–dipole coupling $|\omega_{AB}|$, as shown already by DQC of biradical **1** at X-band frequencies.[5,6] Therefore, the pseudo-secular (flip-flop) term of the dipolar coupling Hamiltonian can be neglected in the analysis of the dipolar evolution functions.[5,6] Orientation selection is not expected to be present in the dipolar evolution functions, as the excitation bandwidth of the 22 ns π-pulse (*ca.* 37 MHz) approximately corresponds to the width of the trityl EPR spectrum (*ca.* 30 MHz), leading to almost full excitation of the spectrum. Hence, all orientations of the vector ***R*** with respect to the vector $\boldsymbol{B}_0$ contribute to the dipolar evolution function with corresponding statistical weights of $\sin(\theta)$. This leads to the well-known Pake pattern in frequency domain with singularities at $\pm D$ and $\pm 2D$. It should be noted that the Pake pattern, corresponding to the DQC time trace, showed somewhat reduced intensity at $\pm 2D$. This is attributed to imperfections in defining the background function, as described below.

Conventional Tikhonov regularisation analysis, with the complete Pake pattern as a kernel function, can be used to analyse the dipolar evolution functions.[26] The mean distances obtained from the distance distribution functions for SIFTER and DQC are 4.9 and 4.86 nm, respectively, (Fig. 3 bottom) which are in good agreement with the data obtained with DQC and PELDOR at X-band.[5,6] Very similar distance distributions were obtained by both SIFTER and DQC. The slight deviations of the mean distances as well as the widths of the distance distribution functions (Fig. 3 bottom) are most probably the result of ambiguities in the definition of the background functions. In the case of single frequency PDS techniques, these functions contain both an interspin and a relaxation-induced component. Thus far, no complete theoretical description exists for these background functions. Hence, the background-correction procedures (described in the Experimental section) were performed similarly to other published work.[23,25]

The raw experimental data for SIFTER and DQC yield different modulation depths. However, due to the different background-correction procedures, it is not possible to compare the modulation depths directly. In order to account for the different modulation depths in the analysis of the signal-to-noise ratios (SNR), it is necessary to scale the raw data to the same range. Thus, the SNR was determined from the standard deviation between the scaled raw experimental time trace and a ninth-order polynomial fit. It was found that, the SNR for SIFTER is approximately four times larger than that for DQC.

PELDOR at G-band frequencies

The EPR spectrum of biradical **1** has a width of 130 MHz at G-band frequencies, this prefers PELDOR experiments to be performed. These experiments have higher sensitivity than corresponding experiments performed on nitroxides. The G-band field-swept Hahn echo-detected EPR spectrum of biradical **1** (Fig. 2), including the pump–probe positions used for the PELDOR experiments, is depicted in Fig. 4.

The background-divided G-band PELDOR time traces obtained at pump–probe positions A, B and C (Fig. 4) show that position A yielded more pronounced high-frequency components, compared to the other two positions. The frequency domain spectrum, obtained by Fourier transformation of the background-divided PELDOR time trace at position A, has the highest intensity at $\pm 2D$ (the shoulders at about ±1 MHz). At this position the detection pulses excite primarily the perpendicular components of the ***g***-tensor ($g_\perp$) of the trityl. Conversely at positions B and C, the detection pulses excite predominantly the parallel components of the ***g***-tensor ($g_{||}$) of the trityl (Fig. 4 upper right). The frequency domain spectra of the time traces B and C show almost vanishingly small intensity at $\pm 2D$ in comparison to the intensity at $\pm D$. These variations of the PELDOR time traces (and corresponding frequency domain patterns) with the resonance positions of the pump and probe pulses indicate the occurrence of orientation selection effects. These effects occur

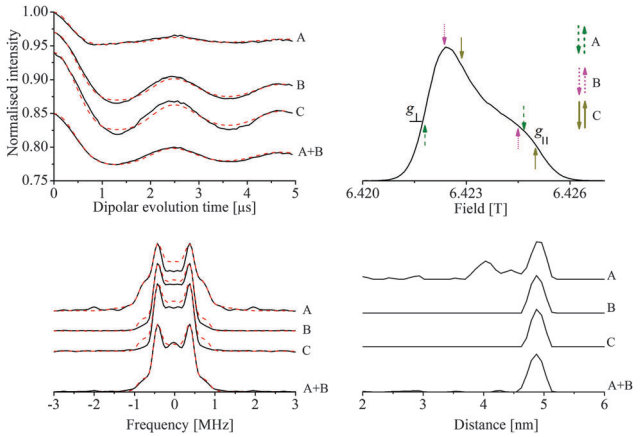

Fig. 4 Left-side (top) – Background-divided PELDOR time traces of biradical **1** obtained at G-band frequencies. Solid lines are experimental data, dashed lines are the fits obtained with Tikhonov regularisation analysis (with a regularisation parameter of 1), as implemented in DeerAnalysis.[26] Positions A, B and C correspond to the positions in the G-band spectrum depicted on the right side. The offset between the probe and pump frequencies is 80 MHz for position A and 60 MHz for positions B and C. The traces obtained at different positions are normalised and vertically shifted for better visual comparison. The raw experimental time traces with the corresponding background functions are shown in Fig. S5 (ESI†). Right-side (top) – Field-swept Hahn echo-detected EPR spectrum obtained at G-band frequencies and a temperature of 25 K depicted with pump–probe positions for PELDOR experiments. Up arrows indicate the detection positions and down arrows indicate the pump positions. Left side (bottom) – Fourier transformation of the background-divided PELDOR time traces. Solid lines are Fourier transformation of the experimental and dashed of the fitted time traces that are obtained with Tikhonov regularisation. The Fourier transformed time traces were normalised and vertically shifted for better visual representation. Positions A, B and C correspond to the positions in the G-band spectrum. Right side (bottom) – Distance distribution functions obtained with Tikhonov regularisation analysis. The distance distribution functions were normalised and vertically shifted for better visual comparison.

due to the partially resolved anisotropy of the ***g***-tensor and excitation of relatively small fractions of the spectrum with the available pulse strengths at G-band frequencies. However, the ***g***-tensor anisotropy is relatively small and combined with weakly defined relative orientations of the trityl moieties (induced by the rotation and bending of the linker segments[6]). This makes the orientation selection effects less pronounced than those seen for tyrosyl[30,31] and nitroxide[32] spin labels rigidly attached to biomolecules. For this reason the weak spectral anisotropy of the PELDOR time traces does not allow us to obtain unambiguous orientational information about the structure of this molecule. The fitting of the PELDOR time traces with a PELDOR database approach[33–36] is given in the ESI.†

The orientation selection effects observed in the three time traces can be understood in terms of the molecular structure and ***g***-tensor orientation. The ***g***-tensor in trityl is orientated with the $g_{||}$ axis perpendicular to the mean linker axis of the molecule. Therefore, when the $g_{||}$ part of the spectrum is sampled (traces B and C), mainly perpendicular orientations of the dipolar coupling tensor are excited. For this reason the PELDOR time traces obtained at positions B and C lack the parallel orientations of the dipolar coupling tensor at $\pm 2D$. However, in the PELDOR time trace obtained at position A (Fig. 4), in which the $g_\perp$ portion of the spectrum is detected, the parallel orientations of the dipolar coupling tensor are excited, giving rise to signal in the frequency pattern at $\pm 2D$. Addition of the time trace at position A to the time trace at position B reduces orientation selection effects further by providing a more uniform excitation of all vector ***R*** orientations with respect to magnetic field vector $\boldsymbol{B}_0$. The frequency domain spectrum of the sum of time traces A and B resembles a full Pake pattern (Fig. 4 bottom left).

Tikhonov analysis of the time traces was performed to generate distance distributions. Analysis of the summed (A + B) time trace yields a distance distribution in good agreement with those obtained from the SIFTER and DQC experiments (and also literature[6]), with a mean distance of 4.88 nm. The distance distribution function at position A reveals a mean distance at about 4.92 nm and additional features probably due to orientation selection effects. However, the distance distribution functions, obtained by Tikhonov regularisation analysis of the time traces at position B and C, reveal only insignificant difference with respect to that obtained by Tikhonov analysis of the A + B time trace (Fig. 4).

Experimental

The concentrations of biradical **1** and monoradical **2** were 200 and 400 μM, respectively, in toluene-d_8 solvent.

Q-band pulsed EPR experiments

Pulsed EPR experiments at Q-band frequencies were performed on a Bruker Elexsys E580 spectrometer, equipped with 10 W AMP-Q-Band solid state amplifier. A more detailed description of the Q-Band setup is given elsewhere.[24] All experiments were performed using the ER5107D2 probe at a temperature of 50 K. For the measurements the samples were transferred into 1 mm inner diameter quartz tubes. To avoid the formation of microcrystals the samples were rapidly frozen in liquid nitrogen before inserting them into the probe. With this setup a π pulse length of 22 ns could be achieved and was used for SIFTER and DQC. The applied SIFTER pulse sequence was $\pi/2\text{–}\tau_1\text{–}\pi\text{–}\tau_1\text{–}\pi/2\text{–}\tau_2\text{–}\pi\text{–}\tau_2$. Unwanted echoes were eliminated by performing a 16 step phase cycle.[23] For the SIFTER time trace a background function was determined by carrying out the experiment on monoradical **2**. The background-correction procedure was performed by a division of the experimental biradical **1** time trace by a Gaussian least-square fit to the monoradical **2** time trace, similarly as performed for SIFTER on nitroxides.[23] The DQC experiment was performed by using the six pulse sequence $\pi/2\text{–}\tau_1\text{–}\pi\text{–}\tau_1\text{–}\pi/2\text{–}\tau_3\text{–}\pi\text{–}\tau_3\text{–}\pi/2\text{–}\tau_2\text{–}\pi\text{–}\tau_2$ and a 64 step phase cycle.[22] τ_3 was kept constant at 35 ns. The background correction for the DQC time trace was performed by a subtraction of a baseline, obtained by an exponential fit function.[25] The raw DQC and SIFTER time traces are depicted in Fig. S4 (ESI†) with the corresponding background functions. For both, DQC and SIFTER experiments τ_1 and τ_2 were changed in 20 ns steps

with initial values of τ_1 = 120 ns and τ_2 = 6000 ns, the microwave frequency was set to the maximum absorption position in the spectrum, the shot repetition time was set to 5000 μs and the measured echo was integrated over 100 ns in 1 ns steps. To suppress deuterium modulations a tau averaging procedure of 8 measurements with steps of $\Delta\tau_1 = \Delta\tau_2$ = 16 ns was performed.

G-band pulsed EPR experiments

Pulsed EPR experiments at G-band frequencies were performed on a home built G-band EPR spectrometer[37,38] at a sample temperature of 25 K. The temperature of 25 K, rather than 50 K, was chosen for pulsed G-band experiments, as an increase of 15 percent in the transversal relaxation time (T_2) was observed at the lower temperature. For the measurements the samples were transferred into 0.4 mm inner diameter tubes. The field-swept Hahn echo-detected EPR spectrum was recorded with pulse lengths of 10 ns and 60 ns (a pulse length of 60 ns corresponds to the flip angle of π) for the first and second pulses, respectively. The length of the first pulse was reduced to 10 ns in order to avoid saturation of the spectrometer receiver by the large signal intensity. For this reason, the shot repetition time was also reduced to 15 ms. The interpulse delay time was set to 200 ns and the number of shots per point was 80. The raw PELDOR time traces are depicted in Fig. S5 (ESI†) with the corresponding exponential background functions. For the G-band PELDOR experiment obtained at position A, the detection pulse lengths were 27.5 ns and 52.5 ns, for the π/2 and π pulses, respectively, and 55 ns for the pump pulse. The initial π/2 and π pulse delay time was 250 ns and kept the same for all PELDOR experiments. The dipolar evolution time window was set to 6.4 μs and the pump–probe frequency offset to 80 MHz. The number of shots per point was 25 and kept the same for all PELDOR experiments; the shot repetition time was 25 ms and the number of scans 51. For the PELDOR experiment obtained at position B the detection pulse lengths were 30 ns and 55 ns, for the π/2 and π pulses, respectively and 50 ns for the pump pulse. The dipolar evolution time window was set to 6.2 μs and the pump–probe frequency offset to 60 MHz. The shot repetition time was 39 ms and the number of scans 55. For the PELDOR experiment obtained at position C the detection pulse lengths were 27.5 ns and 52.5 ns, for the π/2 and π pulses, respectively. The pump pulse length, the dipolar evolution time window and the pump–probe frequency offset were the same as in the case of position B. The shot repetition time was 25 ms and the number of scans 26. The microwave power for the PELDOR experiments was about 60 mW.

Conclusions

SIFTER and DQC experiments at Q-band frequencies and PELDOR experiments at G-band frequencies were performed on a trityl biradical with a known interspin distance of 4.89 nm.[5,6] The narrow spectral width of the trityl biradical of about 30 MHz at Q-band frequencies enabled almost complete excitation of the EPR spectrum with commercially available microwave components. Fulfilment of this condition is necessary for the optimal performance of single frequency dipolar spectroscopy techniques, like SIFTER and DQC. Both methods revealed a distance agreeing with the literature.[5,6] However, the signal-to-noise ratio achieved with SIFTER is about a factor of 4 higher compared to that achieved with DQC. At G-band frequencies the axially symmetric ***g***-tensor anisotropy of the trityl biradical was resolved, preferring the performance of PELDOR experiments. By using Tikhonov regularisation analysis[26] of the averaged PELDOR time trace, the distance that is in agreement with SIFTER and DQC at Q-band frequencies was obtained.

The multi-frequency approach presented here could be useful for biological applications using trityl spin tags on nucleic acids or proteins in cells under physiological conditions.

Acknowledgements

The authors acknowledge Dr Vasyl Denysenkov for the technical support with the G-band EPR spectrometer and Dr Alice Bowen for useful discussions and for proof reading the manuscript. This work is supported by SPP 1601 New Frontiers in Sensitivity for EPR Spectroscopy: from Biological Cells to Nano Materials from the German Research Society DFG, the Cluster of Excellence Frankfurt (CEF) Macromolecular Complexes and the Icelandic Research Fund (120001021), which are all gratefully acknowledged.

References

1 T. J. Reddy, T. Iwama, H. J. Halpern and V. H. Rawal, *J. Org. Chem.*, 2002, **67**, 4635.
2 J. H. Ardenkjær-Larsen, I. Laursen, I. Leunbach, G. Ehnholm, L.-G. Wistrand, J. S. Petersson and K. Golman, *J. Magn. Reson.*, 1998, **133**, 1.
3 G. Y. Shevelev, O. A. Krumkacheva, A. A. Lomzov, A. A. Kuzhelev, O. Y. Rogozhnikova, D. V. Trukhin, T. I. Troitskaya, V. M. Tormyshev, M. V. Fedin, D. V. Pyshnyi and E. G. Bagryanskaya, *J. Am. Chem. Soc.*, 2014, **136**, 9874.
4 Z. Yang, Y. Liu, P. Borbat, J. L. Zweier, J. H. Freed and W. L. Hubbell, *J. Am. Chem. Soc.*, 2012, **134**, 9950.
5 N. C. Kunjir, G. W. Reginsson, O. Schiemann and S. Th. Sigurdsson, *Phys. Chem. Chem. Phys.*, 2013, **15**, 19673.
6 G. W. Reginsson, N. C. Kunjir, S. Th. Sigurdsson and O. Schiemann, *Chem. – Eur. J.*, 2012, **18**, 13580.
7 G. Yu. Shevelev, O. A. Krumkacheva, A. A. Lomzov, A. A. Kuzhelev, D. V. Trukhin, O. Yu. Rogozhnikova, V. M. Tormyshev, D. V. Pyshnyi, M. V. Fedin and E. G. Bagryanskaya, *J. Phys. Chem. B*, 2015, DOI: 10.1021/acs.jpcb.5b03026.
8 R. Owenius, G. R. Eaton and S. S. Eaton, *J. Magn. Reson.*, 2005, **172**, 168.
9 A. J. Fielding, P. J. Carl, G. R. Eaton and S. S. Eaton, *Appl. Magn. Reson.*, 2005, **28**, 231.
10 L. Lumata, Z. Kovacs, A. D. Sherry, C. Malloy, S. Hill, J. van Tol, L. Yu, L. Song and M. E. Merritt, *Phys. Chem. Chem. Phys.*, 2013, **15**, 9800.
11 G. Jeschke, *Annu. Rev. Phys. Chem.*, 2012, **63**, 419.
12 O. Schiemann and T. Prisner, *Q. Rev. Biophys.*, 2007, **40**, 1.

13 A. D Milov, K. M. Salikhov and M. D. Shchirov, *Soviet Physics – Solid State*, 1981, **23**, 565.
14 A. D. Milov, A. B. Ponomarev and Y. D. Tsvetkov, *Chem. Phys. Lett.*, 1984, **110**, 67.
15 M. Pannier, S. Veit, A. Godt, G. Jeschke and H. W. Spiess, *J. Magn. Reson.*, 2000, **142**, 331.
16 R. G. Larsen and D. J. Singel, *J. Chem. Phys.*, 1993, **98**, 5134.
17 W. Hubbell, A. Gross, R. Langen and M. Lietzow, *Curr. Opin. Struct. Biol.*, 1998, **8**, 649.
18 I. Krstic, B. Endeward, D. Margraf, A. Marko and T. F. Prisner, *Top. Curr. Chem.*, 2012, **321**, 159.
19 S. Shelke and S. Sigurdsson, *Struct. Bonding*, 2013, **152**, 121.
20 W. Hubbel, C. Lopez, C. Altenbach and Z. Yang, *Curr. Opin. Struct. Biol.*, 2013, **23**, 725.
21 G. Fanucci and D. Cafiso, *Curr. Opin. Struct. Biol.*, 2006, **16**, 644.
22 P. P. Borbat and J. H. Freed, *Chem. Phys. Lett.*, 1999, **313**, 145.
23 G. Jeschke, M. Pannier, A. Godt and H. W. Spiess, *Chem. Phys. Lett.*, 2000, **331**, 243.
24 P. Schöps, P. E. Spindler, A. Marko and T. F. Prisner, *J. Magn. Reson.*, 2015, **250**, 55.
25 P. Borbat, H. Mchaourab and J. Freed, *J. Am. Chem. Soc.*, 2002, **124**, 5304.
26 G. Jeschke, V. Chechik, P. Ionita, A. Godt, H. Zimmermann, J. Banham, C. Timmel, D. Hilger and H. Jung, *Appl. Magn. Reson.*, 2006, **30**, 473.
27 D. Banerjee, J. C. Paniagua, V. Mugnaini, J. Veciana, A. Feintuch, M. Pons and D. Goldfarb, *Phys. Chem. Chem. Phys.*, 2011, **13**, 18626.
28 B. D. Armstrong, D. T. Edwards, R. J. Wylde, S. A. Walker and S. Han, *Phys. Chem. Chem. Phys.*, 2010, **12**, 5920.
29 J. H. Ardenkjær-Larsen, S. Macholl and H. Johannesson, *Appl. Magn. Reson.*, 2008, **34**, 509.
30 V. Denysenkov, T. Prisner, J. Stubbe and M. Bennati, *Proc. Natl. Acad. Sci. U. S. A.*, 2006, **103**, 13386.
31 V. P. Denysenkov, D. Biglino, W. Lubitz, T. F. Prisner and M. Bennati, *Angew. Chem., Int. Ed.*, 2008, **47**, 1224.
32 A. Marko, V. P. Denysenkov, D. Margraf, P. Cekan, O. Schiemann, S. T. Sigurdsson and T. F. Prisner, *J. Am. Chem. Soc.*, 2011, **133**, 13375.
33 A. Marko and T. F. Prisner, *Phys. Chem. Chem. Phys.*, 2013, **15**, 619.
34 T. F. Prisner, A. Marko and S. Th. Sigurdsson, *J. Magn. Reson.*, 2015, **252**, 187.
35 D. Abdullin, G. Hagelueken, R. I. Hunter, G. M. Smith and O. Schiemann, *Mol. Phys.*, 2015, **113**, 544.
36 C. Abe, D. Klose, F. Dietrich, W. H. Ziegler, Y. Polyhach, G. Jeschke and H.-J. Steinhoff, *J. Magn. Reson.*, 2012, **216**, 53.
37 M. Rohrer, O. Brügman, B. Kinzer and T. Prisner, *Appl. Magn. Reson.*, 2001, **21**, 257.
38 V. Denysenkov, T. Prisner, J. Stubbe and M. Bennati, *Appl. Magn. Reson.*, 2005, **29**, 375.

